THE EUROPEAN
PHYSICAL JOURNAL C

Cosmological constraints on $\Lambda(t)$CDM models

H. A. P. Macedo[1,a] , **L. S. Brito**[1,b] , **J. F. Jesus**[1,2,c] , **M. E. S. Alves**[1,3,d]

[1] Universidade Estadual Paulista (UNESP), Faculdade de Engenharia e Ciências, Departamento de Física, Av. Dr. Ariberto Pereira da Cunha 333, Guaratinguetá, SP 12516-410, Brazil
[2] Universidade Estadual Paulista (UNESP), Instituto de Ciências e Engenharia, Departamento de Ciências e Tecnologia, R. Geraldo Alckmin, 519, Itapeva, SP 18409-010, Brazil
[3] Universidade Estadual Paulista (UNESP), Instituto de Ciência e Tecnologia, São José dos Campos, SP 12247-004, Brazil

Abstract Problems with the concordance cosmology ΛC DM as the cosmological constant problem, coincidence problems and Hubble tension has led to many proposed alternatives, as the $\Lambda(t)$CDM, where the now called Λ cosmological term is allowed to vary due to an interaction with pressureless matter. Here, we analyze one class of these proposals, namely, $\Lambda = \alpha' a^{-2} + \beta H^2 + \lambda_*$, based on dimensional arguments. Using SNe Ia, cosmic chronometers data plus constraints on H_0 from SH0ES and Planck satellite, we constrain the free parameters of this class of models. By using the Planck prior over H_0, we conclude that the λ_* term can not be discarded by this analysis, thereby disfavouring models only with the time-variable terms. The SH0ES prior over H_0 has an weak evidence in this direction. The subclasses of models with $\alpha' = 0$ and with $\beta = 0$ can not be discarded by this analysis. Finally, by using distance priors from CMB, the Λ time-dependence was quite restricted.

1 Introduction

The concordance cosmological model ΛCDM (Λ plus Cold Dark Matter) is very successful in explaining a variety of cosmological observations as, for instance, the accelerating expansion of the Universe and the power spectrum of the cosmic microwave background radiation (CMB). However, the model suffers several theoretical and observational difficulties. Some remarkable examples are the cosmological constant problem, the coincidence problem, and the Hubble tension (see, e.g., [1] for a review).

[a] e-mail: ha.macedo@unesp.br (corresponding author)

[b] e-mail: lucas.s.brito@unesp.br

[c] e-mail: jf.jesus@unesp.br

[d] e-mail: marcio.alves@unesp.br

In the last decades, we have seen an increasing number of alternatives to the ΛCDM model aiming to alleviate such difficulties. These alternatives range from the quest for dark energy models to extended theories of gravity. In this context, it is natural to investigate if Λ is a function of the cosmic time t.

Models with a time-varying Λ or Vacuum-decay models have been conceived in different contexts. In several models, some ad hoc time dependence for $\Lambda(t)$ is assumed. Some of the most common examples were addressed in Refs. [2,3] (see [4] and references therein for a list of phenomenological decay laws of $\Lambda(t)$). The functional form of $\Lambda(t)$ can also be derived, for instance, by geometrical motivations [5,6] or from Quantum Mechanical arguments [7]. The interaction of vacuum with matter has also been considered in different approaches and confronted with recent cosmological data (see, e.g., [8–11]).

A promising approach to overcome the puzzles of the ΛCDM model is known as the 'running vacuum model' (RVM). It emerges when one uses the renormalization group approach of quantum field theory in curved spaces to renormalize the vacuum energy density. It is possible to show that vacuum energy density evolves as a series of powers of the Hubble function H and its derivatives with respect to cosmic time: $\rho_{\rm vac}(H, \dot{H}, \ldots)$. The leading term of the expansion is constant, but the next-to-leading one evolves as H^2. There are other terms in the expansion that can be relevant for the early Universe cosmology, but the term H^2 can affect the current evolution of the scale factor. Initially, the RVM was introduced in a semi-qualitative way through the renormalization group approach. Some of the first motivations of this model can be found, e.g., in the Refs. [12–15] (see also [16] for an old review on the subject). However, in recent years, the RVM was derived from a rigorous analysis within the Quantum Field Theory in curved spacetime. The derivation

of the final form of RVM can be found in the Refs. [17–20] (see [21] for a review on recent theoretical developments). Moreover, such a class of models can be more favored than the ΛCDM model when a fit with the cosmological observables is performed [22–28].

To answer the conundrum of why the cosmological constant is so small today, one could also propose models with $\Lambda \propto a^{-m}$, where a is the scale factor and m is a positive constant to be determined. From dimensional arguments by quantum cosmology, it is natural to choose $m = 2$ [29,30]. Therefore, in this perspective, Λ has the same decay behavior as the curvature term. Such an evolution of Λ was first proposed by özer and Taha [31,32] as a way to solve the cosmological problems of the eighties decade.

On the other hand, following similar phenomenological arguments, in Ref. [33], the authors parametrized the time evolution of Λ as the sum of a term proportional to a^{-2} to a term proportional to H^2, i.e., the same term that emerges from the RVM. In the present article, we follow this approach, but we add a "bare" cosmological term λ_*. Specifically, we consider four models of a time-varying $\Lambda(t)$ in the class

$$\Lambda_g = \frac{\alpha'}{a^2} + \beta H^2 + \lambda_*, \tag{1}$$

with α', β and λ_* constants. Three models are chosen by selecting one of these constants to vanish identically (these three models are depicted in Table 1) and the fourth model is the complete one for which the three constants are non-null.

The phenomenological model described by the complete model presents a smooth transition from the early de Sitter stage to the radiation phase. Such a transition is independent of the curvature parameter and solves naturally the horizon and the graceful exit problem [34].

To put constraints on the free parameters of the models, we use the SNe Ia sample consisting of 1048 SNe Ia apparent magnitude measurements from the Pantheon sample [35] and a compilation of 32 cosmic chronometers data of the Hubble parameter, $H(z)$ [36]. We have also considered the most up-to-date constraints on H_0, namely, the ones from SH0ES [37] and Planck [38].

We organized the article as follows. We describe the Friedmann equations with a time-dependent $\Lambda(t)$-term in Sect. 2 (neglecting radiation) and Sect. 3 (including radiation). We

obtain analytical solutions for $H(z)$ in the class of models given by Eq. (1) in Sects. 2.1 and 3.1. In Sect. 4, we constrain the parameters of the models using SNe Ia data, cosmic chronometers data and CMB. In the analysis, we consider separately the constraints on H_0 from Planck (Sect. 4.1) and from SH0ES (Sect. 4.2). Finally, we present our conclusions and final remarks in Sect. 5.

2 Cosmological equations for a varying ΛL term, neglecting radiation

From the Cosmological Principle and the Einstein Field Equations, we have the so-called Friedmann equations, given by

$$H^2 = \frac{8\pi G \rho_T}{3} - \frac{k}{a^2}, \tag{2}$$

$$\frac{\ddot{a}}{a} = -\frac{4\pi G}{3}(\rho_T + 3p_T), \tag{3}$$

where ρ_T is the total density of the Universe matter-energy content, p_T is total pressure and k is the curvature scalar. As we are mainly interested in the late-time Universe, we shall neglect the radiation contribution, in such a way that ρ_T is given by

$$\rho_T = \rho_M + \rho_\Lambda, \tag{4}$$

where ρ_M corresponds to the total pressureless matter (dark matter+baryons) and ρ_Λ corresponds to the time-varying $\Lambda(t)$-term. In the present article we assume the equation of state (EoS) of vacuum to be exactly $w_{vac} = -1$ such that $p_\Lambda = -\rho_\Lambda$. However, a recent result for the RVM is that the EoS of vacuum evolves with the cosmic history [19]. This would change our results and may be considered in future works. From the continuity equation, we have

$$\dot{\rho}_M + 3H\rho_M = Q, \tag{5}$$

$$\dot{\rho}_\Lambda = -Q, \tag{6}$$

where Q is the interaction term between pressureless matter and vacuum. With these components, the Friedmann equations (3) now read

$$H^2 = \frac{8\pi G(\rho_M + \rho_\Lambda)}{3} - \frac{k}{a^2}, \tag{7}$$

$$\frac{\ddot{a}}{a} = -\frac{4\pi G}{3}(\rho_M - 2\rho_\Lambda). \tag{8}$$

By multiplying the Eq. (8) by 2, we have

$$2\frac{\ddot{a}}{a} = -\frac{8\pi G}{3}(\rho_M - 2\rho_\Lambda) = -\frac{8\pi G}{3}\rho_M + \frac{16\pi G}{3}\rho_\Lambda, \tag{9}$$

Table 1 Here we summarise the three models considered in the article

Model	Λ	Fixed parameter
Λ_1	$\frac{\alpha'}{a^2} + \beta H^2$	$\lambda_* = 0$
Λ_2	$\frac{\alpha'}{a^2} + \lambda_*$	$\beta = 0$
Λ_3	$\beta H^2 + \lambda_*$	$\alpha' = 0$

and summing the Eq. (7) with the Eq. (9), we have

$$H^2 + \frac{2\ddot{a}}{a} = 8\pi G\rho_\Lambda - \frac{k}{a^2}. \tag{10}$$

Since $\Lambda = 8\pi G\rho_\Lambda$, Eq. (10) reads

$$H^2 = -\frac{2\ddot{a}}{a} + \Lambda - \frac{k}{a^2}. \tag{11}$$

By replacing $\frac{\ddot{a}}{a} = \dot{H} + H^2$, we find

$$3H^2 = -2\dot{H} + \Lambda - \frac{k}{a^2}. \tag{12}$$

In order to perform cosmological constraints, let us now change to derivatives with respect to the redshift

$$\frac{d}{dt} = -H(1+z)\frac{d}{dz}. \tag{13}$$

Thus, the equation

$$2\dot{H} = -3H^2 + \Lambda - \frac{k}{a^2}, \tag{14}$$

now reads

$$-2H(1+z)\frac{dH}{dz} = -3H^2 + \Lambda - \frac{k}{a^2}, \tag{15}$$

and by replacing $k = -\Omega_{k0}H_0^2$ we have

$$\frac{dH}{dz} = \frac{3H}{2(1+z)} - \frac{\Omega_{k0}H_0^2(1+z)}{2H} - \frac{\Lambda}{2H(1+z)}. \tag{16}$$

If we further use the definition $E \equiv \frac{H}{H_0}$ the above equation reads

$$\frac{dE}{dz} = \frac{3E}{2(1+z)} - \frac{\Omega_{k0}(1+z)}{2E} - \frac{\Lambda}{2EH_0^2(1+z)}. \tag{17}$$

From now on, we shall assume that the Universe is spatially flat ($k = 0$), as indicated by inflation and CMB. Therefore, we finally obtain the equation

$$\frac{dE}{dz} = \frac{3E}{2(1+z)} - \frac{\Lambda}{2EH_0^2(1+z)}. \tag{18}$$

For a given $\Lambda(a, H)$ (or $\Lambda(z, H)$), Eq. (18) can be solved in order to obtain the universe evolution $E(z)$. In the next subsection, we shall assume a fair general $\Lambda(a, H)$ dependence in order to solve this equation and compare the assumed models with cosmological observations.

2.1 $\Lambda = \alpha' a^{-2} + \beta H^2 + \lambda_*$ class of models, neglecting radiation

Dimensional arguments have led to the proposals of $\Lambda \propto a^{-2}$, $\Lambda \propto H^2$ models in the literature. Here we test a combination of these proposals together with a constant term, in order to find which of these terms may contribute the most to the evolution of the universe as indicated by observations.

So, the models we study here are derived from the following Λ dependence

$$\Lambda_g = \frac{\alpha'}{a^2} + \beta H^2 + \lambda_*. \tag{19}$$

We shall not consider this general Λ_g as a model to be constrained by observations, as it has too many free parameters, and it may be penalized in a Bayesian criterion. Actually, we choose to work with particular cases of this Λ_g dependence, where, in each case, one parameter contribution is neglected, as summarised in Table 1.

Let us now obtain the evolution of this class of models. From Eq. (19), we have the values today

$$\Lambda_0 = \alpha' + \beta H_0^2 + \lambda_*. \tag{20}$$

As $\Omega_\Lambda \equiv \frac{\Lambda_0}{3H_0^2}$, we may also write

$$\Omega_\Lambda = \frac{\alpha}{3} + \frac{\beta}{3} + \frac{\lambda_*}{3H_0^2} = \frac{\alpha}{3} + \frac{\beta}{3} + \Omega_{\lambda*}, \tag{21}$$

where we have defined $\Omega_{\lambda*} \equiv \frac{\lambda_*}{3H_0^2}$ and the dimensionless $\alpha \equiv \frac{\alpha'}{H_0^2}$, for mathematical convenience. From this, we may write for α

$$\alpha = 3\left(\Omega_\Lambda - \frac{\beta}{3} - \Omega_{\lambda*}\right). \tag{22}$$

As already mentioned, we choose to work with a spatially flat Universe, such that from Eq. (7), we have the normalization condition

$$\Omega_\Lambda = 1 - \Omega_m. \tag{23}$$

Now, with these dimensionless parameters ($\Omega_m, \beta, \Omega_{\lambda*}$), an analytical solution for the Eq. (18) can be obtained. The general solution is given by

$$E^2(z) = \left[\frac{6\Omega_{\lambda*} + (3-\beta)(1-3\Omega_\Lambda)}{(1-\beta)(3-\beta)}\right](1+z)^{3-\beta} + \frac{3\Omega_{\lambda*}}{3-\beta} + \left[\frac{-3\Omega_{\lambda*} + 3\Omega_\Lambda - \beta}{1-\beta}\right](1+z)^2. \tag{24}$$

The solutions for each one of the three models depicted in the Table 1 are particular cases of this solution obtined by the appropriate choice of parameters. They are given by

- Model $\Lambda_1 = \frac{\alpha'}{a^2} + \beta H^2$, ($\lambda_* = 0$)

$$E(z) = \sqrt{\frac{1 - 3\Omega_\Lambda}{1-\beta}(1+z)^{(3-\beta)} + \frac{3\Omega_\Lambda - \beta}{1-\beta}(1+z)^2}; \tag{25}$$

- Model $\Lambda_2 = \frac{\alpha'}{a^2} + \lambda_*$, ($\beta = 0$)

$$E(z) = \sqrt{(1 + 2\Omega_{\lambda*} - 3\Omega_\Lambda)(1+z)^3 + \Omega_{\lambda*} + 3(-\Omega_{\lambda*} + \Omega_\Lambda)(1+z)^2}; \tag{26}$$

- Model $\Lambda_3 = \beta H^2 + \lambda_*$, $(\alpha' = 0)$

$$E(z) = \sqrt{\left[\frac{6\Omega_{\lambda_*} + (3-\beta)(1-3\Omega_\Lambda)}{(1-\beta)(3-\beta)}\right](1+z)^{3-\beta} + \frac{3\Omega_{\lambda_*}}{3-\beta}}. \quad (27)$$

It is worth noticing that, for the Λ_2 model, the $E(z)$ given by Eq. (26) is similar to the ΛCDM model with spatial curvature. This is due to the fact that the term $\propto a^{-2}$ mimics a curvature term in this case.

The functions $E(z)$ we have obtained are all we need in order to constrain the three models with observational data in the next section. We can also obtain the interaction term for each model, in order to analyze its behavior later. For the general case (19), we have the following interaction term

$$\mathcal{Q}(z) \equiv \frac{8\pi G}{H_0^3} Q(z) = 2\alpha(1+z)^2 E(z)$$

$$+ \beta E(z)(1+z)\frac{dE^2(z)}{dz}. \quad (28)$$

3 Cosmological equations for a varying Λ term, including radiation

Taking radiation into account, the Friedmann equations (3) are the same, but now we have ρ_T and p_T given by:

$$\rho_T = \rho_M + \rho_r + \rho_\Lambda \quad (29)$$

$$p_T = p_r + p_\Lambda = \frac{\rho_r}{3} - \rho_\Lambda \quad (30)$$

where ρ_r is radiation density and $\rho_M = \rho_d + \rho_b$ (dark matter (d)+baryons (b)). The continuity equations now read

$$\dot{\rho}_b + 3H\rho_b = 0, \quad (31)$$

$$\dot{\rho}_r + 4H\rho_r = 0, \quad (32)$$

$$\dot{\rho}_d + 3H\rho_d = Q, \quad (33)$$

$$\dot{\rho}_\Lambda = -Q, \quad (34)$$

where Q is the interaction term between dark matter and vacuum. It is interesting to note that Eqs. (31) and (33) can be combined to write a continuity equation for total pressureless matter:

$$\dot{\rho}_M + 3H\rho_M = Q \quad (35)$$

With these components, the Friedmann equations (3) now read

$$H^2 = \frac{8\pi G(\rho_M + \rho_r + \rho_\Lambda)}{3} - \frac{k}{a^2}, \quad (36)$$

$$\frac{\ddot{a}}{a} = -\frac{4\pi G}{3}(\rho_M + 2\rho_r - 2\rho_\Lambda). \quad (37)$$

It can be shown, that following the same steps as in Sect. 2, we may arrive at the general result, with spatial curvature:

$$\frac{dE}{dz} = \frac{3E}{2(1+z)} - \frac{\Omega_{k0}(1+z)}{2E} + \frac{\Omega_{r0}(1+z)^3}{2E} - \frac{\Lambda}{2EH_0^2(1+z)}. \quad (38)$$

And, by assuming that the Universe is spatially flat ($k = 0$), as indicated by inflation and CMB, we obtain the equation:

$$\frac{dE}{dz} = \frac{3E}{2(1+z)} + \frac{\Omega_{r0}(1+z)^3}{2E} - \frac{\Lambda}{2EH_0^2(1+z)}. \quad (39)$$

For a given $\Lambda(a, H)$ (or $\Lambda(z, H)$), Eq. (39) can be solved in order to obtain the universe evolution $E(z)$. In the next subsection, we assume the same $\Lambda(a, H)$ dependence as before (19) in order to solve this equation and compare the assumed models with cosmological observations.

3.1 $\Lambda = \alpha' a^{-2} + \beta H^2 + \lambda_*$ class of models, including radiation

For this class, including radiation, the normalization condition now reads:

$$\Omega_\Lambda = 1 - \Omega_m - \Omega_r. \quad (40)$$

Now, with the dimensionless parameters (Ω_m, Ω_r, α, β, Ω_{λ_*}), an analytical solution for the Eq. (18) can be obtained. The general solution is given by

$$E^2(z) = \frac{(1+z)^{3-\beta}}{3-\beta}\left(\frac{2\alpha}{\beta-1} + 3\Omega_{m0} + \frac{4\beta\Omega_{r0}}{1+\beta}\right)$$

$$+ \frac{\Omega_{r0}(1+z)^4}{(1+\beta)} + \frac{\alpha(1+z)^2}{(1-\beta)} + \frac{3\Omega_{\lambda_*}}{3-\beta} \quad (41)$$

which is a general solution in the cases that $\beta \notin \{-1, 1, 3\}$.

4 Analysis and results

For this analysis, we use 3 variations of the general equation, being first with $\lambda_* = 0$, second with $\beta = 0$, and last we take $\alpha = 0$, as described in Table 1.

In order to constrain the models in the present work, we have used as observational data, the SNe Ia sample consisting of 1048 SNe Ia apparent magnitude measurements from the Pantheon sample [35] and a compilation of 32 Hubble parameter data, $H(z)$ [36], obtained by estimating the differential ages of galaxies, called Cosmic Chronometers (CCs).

The 32 $H(z)$ CCs data is a sample compiled by [36], consisting of $H(z)$ data within the range $0.07 < z < 1.965$. In the Ref. [36], the authors have estimated systematic errors for these data, by running simulations and considering effects
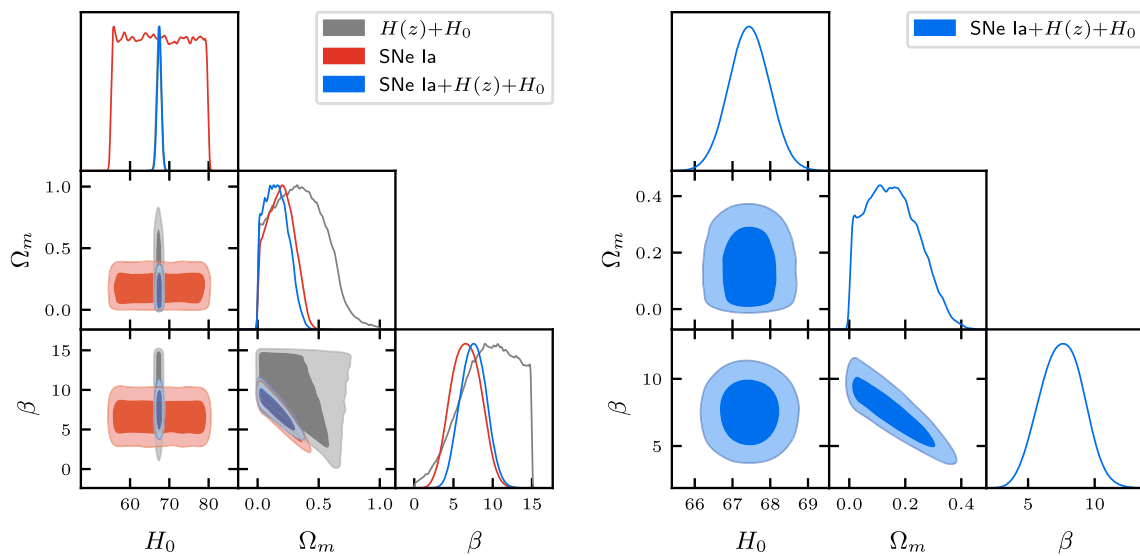
Fig. 1 SNe Ia, $H(z)$ and Planck H_0 constraints for $\lambda_* = 0$ (Λ_1 model), at 1 and 2σ c.l., H_0 units are km/s/Mpc. Left: SNe Ia, $H(z)$+Planck H_0 and SNe Ia+$H(z)$+Planck H_0 constraints. Right: joint constraints from SNe Ia+$H(z)$+Planck H_0

such as metallicity, rejuvenation effect, star formation history, initial mass function, choice of stellar library etc.[1]

The Pantheon compilation consists of 1048 data from SNe Ia, within the redshift range $0.01 < z < 2.3$, containing measurements of SDSS, Pan-STARRS1 (PS1), SDSS, SNLS, and various HST and low-z datasets.

In order to better constrain the models, besides SNe Ia+$H(z)$ data, we have also considered the most up-to-date constraints over H_0, namely, the ones from SH0ES (73.2 ± 1.3) km/s/Mpc [37] and Planck (67.36 ± 0.54) km/s/Mpc [38]. As it is well known, these constraints are currently in conflict, generating the so-called "H_0 tension" [39]. It is important to mention that these constraints are obtained from quite different methods. While the SH0ES H_0 is obtained simply from local constraints, following the distance ladder built from Cepheid distances and local SNe Ia, the Planck H_0 is obtained from high redshift constraints, assuming the flat ΛCDM model. Given this tension, we preferred to make two separate analyses, one considering the H_0 from Planck and one taking into account the H_0 from SH0ES.

Below, we show the results of our analyses, first showing the constraints from SNe Ia+$H(z)$+H_0 from Planck, and later showing the constraints from SNe Ia+$H(z)$+H_0 from SH0ES.

In all the analyses that we have made, we have assumed the flat priors over the free parameters: $\alpha \in [-2, 2]$, $\beta \in [-5, 15]$, $\Omega_m \in [0, 1]$, $H_0 \in [55, 85]$ km/s/Mpc. It is important to note that while SNe Ia data constrain $\{\Omega_m, \alpha, \beta\}$, $H(z)$

Table 2 SNe Ia+$H(z)$+Planck H_0 constraints for $\lambda_* = 0$ (Λ_1 model)

| Parameter	95% limits
H_0 (km/s/Mpc)	67.4 ± 1.1
Ω_m	$0.15^{+0.16}_{-0.15}$
β	$7.5^{+3.2}_{-3.1}$

data constrain $\{H_0, \Omega_m, \alpha, \beta\}$. However, $H(z)$ data alone do not provide strong constraints over the free parameters, so we choose to work with $H(z)$+SNe Ia data combination. Furthermore, we have added constraints over H_0 from Planck and SH0ES in order to probe the H_0 tension and also because they consist of strong constraints over H_0.

4.1 SNe Ia+$H(z)$+Planck H_0 analysis

We start with the Λ_1 model (see Table 1). As one may see in Fig. 1 (left), H_0 is well constrained by $H(z)$+Planck H_0 data, but Ω_m and β are poorly constrained. In fact, one may see that Ω_m is constrained by the prior in its inferior limit, while β is constrained by the prior in its superior limit. H_0 can not be constrained by SNe Ia, but β is well constrained by this data. Ω_m is better constrained by SNe Ia, but also is constrained inferiorly by the prior. In Fig. 1 (right), we can see the result for the joint analysis, where Ω_m and β are better constrained, although Ω_m yet is constrained inferiorly by the prior. We show the best-fit values for the parameters of the Λ_1 model in Table 2.

In Fig. 2 we show the analysis for the Λ_2 model ($\beta = 0$). As one can see in the left panel, $H(z)$+Planck H_0 data constrains well H_0 and α, but not Ω_m, which is constrained
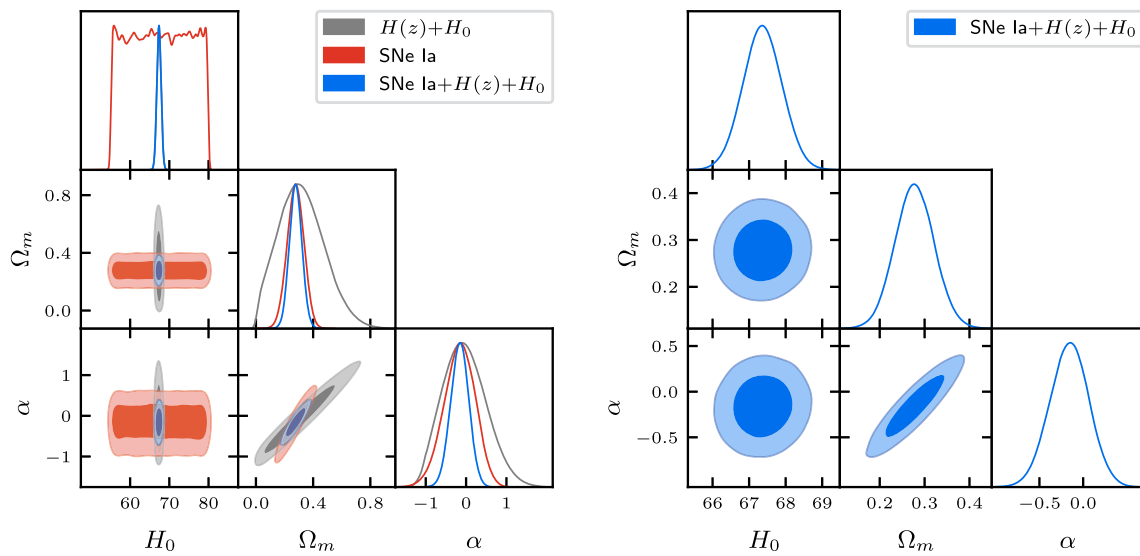
Fig. 2 SNe Ia, $H(z)$ and Planck H_0 constraints for $\beta = 0$ (Λ_2 model), at 1 and 2σ c.l., H_0 units are km/s/Mpc. Left: SNe Ia, $H(z)$+Planck H_0 and SNe Ia+$H(z)$+Planck H_0 constraints. Right: joint constraints from SNe Ia+$H(z)$+Planck H_0

Table 3 SNe Ia+$H(z)$+Planck H_0 constraints for $\beta = 0$ (Λ_2 model)

| Parameter	95% limits
H_0 (km/s/Mpc)	67.4 ± 1.1
Ω_m	$0.278^{+0.088}_{-0.086}$
α	$-0.16^{+0.44}_{-0.45}$

by the prior in its inferior limit. As SNe Ia does not constrain H_0, but Ω_m and α are well constrained by this data, it is interesting to combine SNe Ia and $H(z)$ data. One may see

in Fig. 2 (right) and Table 3, the result for the joint analysis, where H_0, Ω_m and α are better constrained.

Next, we analyze the Λ_3 model ($\alpha = 0$) for which we also put constraints on the parameters $\{H_0, \Omega_m, \beta\}$. In Fig. 3 (left), we can see that H_0 and β are well constrained by $H(z)$+Planck H_0 data, while Ω_m is weakly constrained. Ω_m and β are well constrained by SNe Ia, thus complementing the $H(z)$+Planck H_0 data constraints. In Fig. 3 (right) and Table 5, we highlight the result for the joint analysis, where H_0, Ω_m, and β are better constrained.

From Fig. 4 (upper panel), one may notice that in the past ($z \gtrsim 0.3$) the interaction term was positive, meaning a vac-
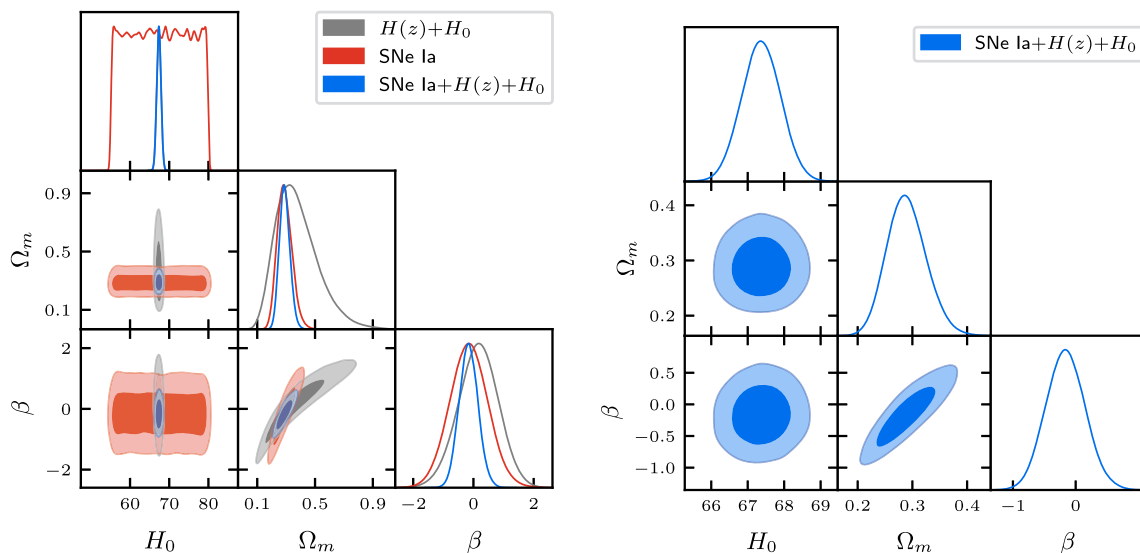
Fig. 3 SNe Ia, $H(z)$ and Planck H_0 constraints for $\alpha = 0$ (Λ_3 model), at 1 and 2σ c.l., H_0 units are km/s/Mpc. Left: SNe Ia, $H(z)$+Planck H_0 and SNe Ia+$H(z)$+ Planck H_0 constraints. Right: SNe Ia+$H(z)$+Planck H_0 joint constraints
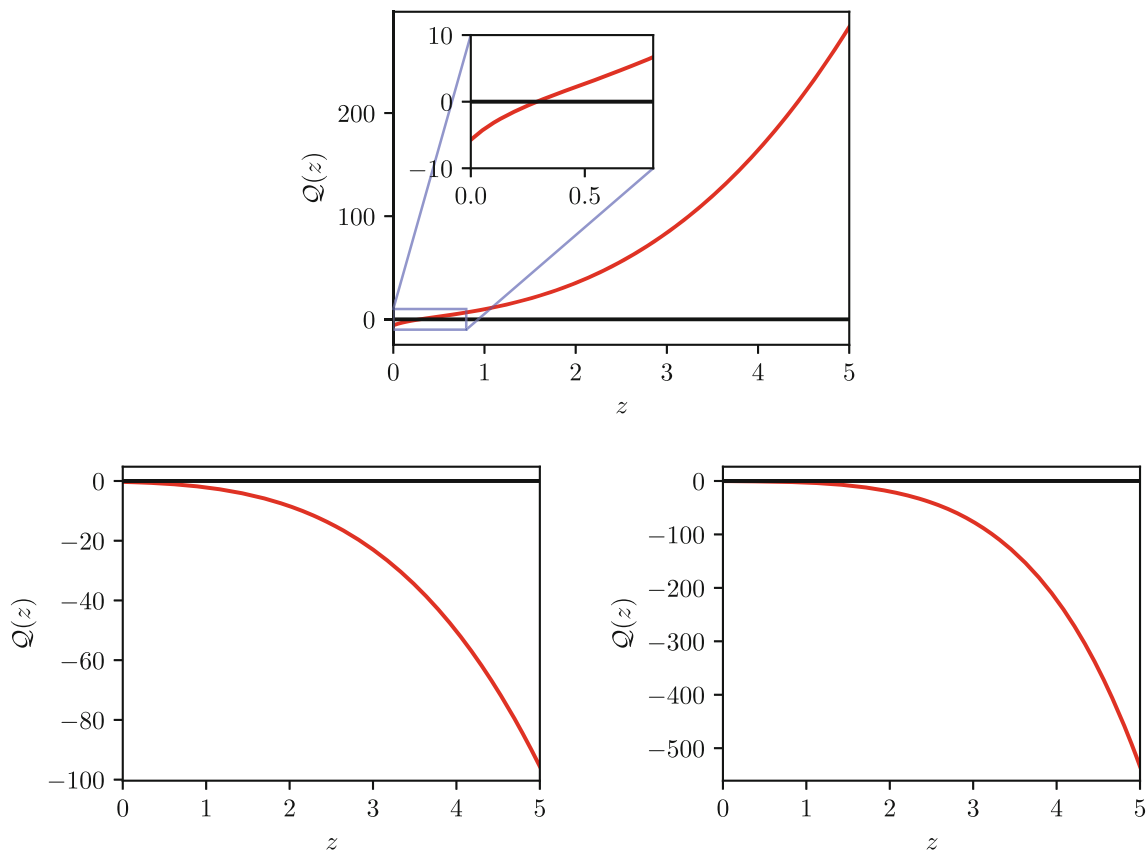
Fig. 4 Interaction term $\mathcal{Q}(z)$ for the best fit parameters from SNe Ia+$H(z)$+H_0 from Planck. Upper panel: $\lambda_* = 0$ (Λ_1 model). Bottom left: $\beta = 0$ (Λ_2 model). Bottom right: $\alpha = 0$ (Λ_3 model)
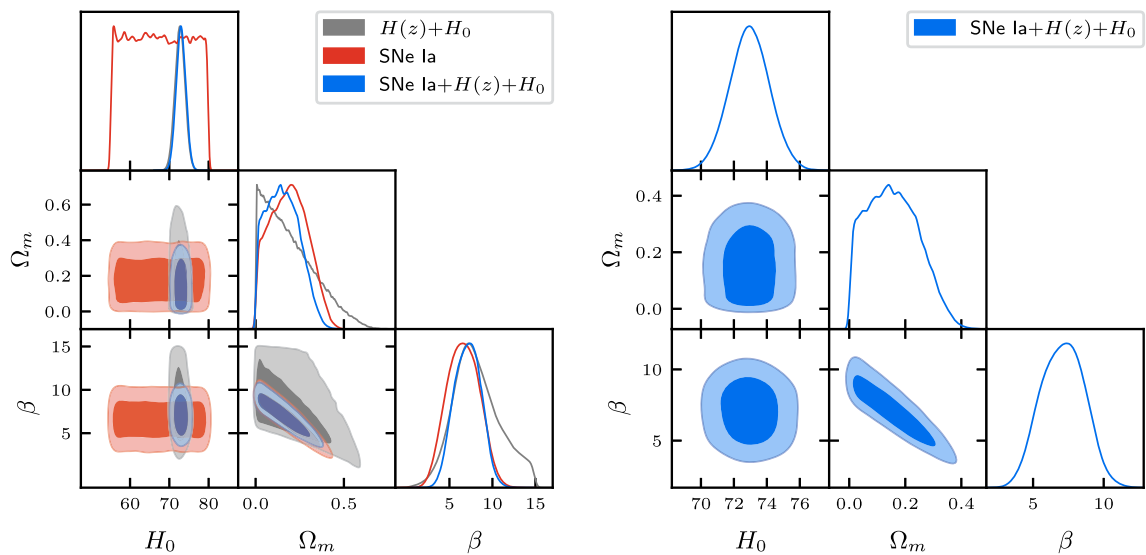
Fig. 5 SNe Ia+$H(z)$+H_0 from SH0ES for $\lambda_* = 0$ (Λ_1 model), at 1 and 2σ c.l., H_0 units are km/s/Mpc. Left: SNe Ia, $H(z)$+SH0ES H_0 and SNe Ia+$H(z)$+H_0 from SH0ES constraints. Right: SNe Ia+$H(z)$+H_0 from SH0ES joint constraints

uum decaying into DM. However, it is interesting that, for this model (Λ_1), the interaction term changes sign at low redshift, indicating that now we have decaying of DM into Λ. This is due to the fact that $\beta > 0$ and $\alpha < 0$ in the best fit,

leading to a change of sign of $\mathcal{Q}(z)$, as one may see from Eq. (28). For Λ_2 and Λ_3 models, however, the interaction term is always negative, thus indicating a decaying of DM into Λ. We may conclude that, at least for the best-fit models, that

Table 4 SNe Ia+$H(z)$+SH0ES H_0 constraints for $\lambda_* = 0$ (Λ_1 model)

Parameter	95% limits
H_0 (km/s/Mpc)	$73.0^{+2.4}_{-2.4}$
Ω_m	$0.16^{+0.16}_{-0.15}$
β	$7.1^{+3.0}_{-2.9}$

Table 5 SNe Ia+$H(z)$+Planck H_0 constraints for $\alpha = 0$ (Λ_3 model)

Parameter	95% limits
H_0 (km/s/Mpc)	67.4 ± 1.1
Ω_m	$0.290^{+0.076}_{-0.067}$
β	$-0.16^{+0.64}_{-0.61}$

Table 6 SNe Ia+$H(z)$+ SH0ES H_0 constraints for $\beta = 0$ (Λ_2 model)

Parameter	95% limits
H_0 (km/s/Mpc)	$72.7^{+2.5}_{-2.5}$
Ω_m	$0.289^{+0.085}_{-0.084}$
α	$-0.03^{+0.42}_{-0.43}$

Λ_1 is the only model that alleviates or solves the Cosmological Constant Problem (CCP). However, as one can see from Tables 2 and 3, α and β may have positive values within 95% c.l., thus allowing also for decaying of Λ into DM. For Λ_1, however, there is not such a change of tendency when we change the values of α and β within 95% c.l.

4.2 SNe Ia+$H(z)$+SH0ES H_0 analysis

In Fig. 5, we may see the constraints from SNe Ia, $H(z)$ data and H_0 from SH0ES over the model Λ_1 (with $\lambda_* = 0$).

As one may see in Fig. 5 (left), $H(z)$+SH0ES H_0 data constrains well H_0, but not Ω_m, as it is being constrained by the prior in its inferior limit, while β is constrained by the prior in its superior limit. H_0 is not constrained by SNe Ia, but Ω_m and β are better constrained by this data. In Fig. 5

(right), we can see the result for the joint analysis, where Ω_m and β are better constrained, although Ω_m still is constrained by the prior in its inferior limit. The best-fit values for the Λ_1 model in this case are shown in Tables 4 and 5.

In Fig. 6, we may see the constraints from SNe Ia, $H(z)$ data and H_0 from SH0ES over the model Λ_2 (with $\beta = 0$).

In Fig. 6 (left), $H(z)$ data constrains well H_0 and α, but not Ω_m, which is constrained by the prior in its inferior limit. H_0 is not constrained by SNe Ia, but Ω_m and α are well constrained by this data. In Fig. 6 (right) and in Table 6, we can see the result for the joint analysis, where Ω_m and β are better constrained. We may see that H_0, Ω_m and α are well constrained by this analysis.

Below, in Fig. 7, we may see the constraints from SNe Ia, $H(z)$ data and H_0 from SH0ES over the model Λ_3 (with $\alpha = 0$).

We can see in Fig. 7 (left), $H(z)$+SH0ES H_0 data constraints well H_0 and β, but not Ω_m, which is being constrained by the prior in its inferior limit. H_0 is not constrained by SNe Ia, but Ω_m and β are well constrained by this data. One may see in Fig. 7 (right), the result for the joint analysis, where H_0, Ω_m, and β are well constrained. In Table 7 we show the best-fit values for this model.
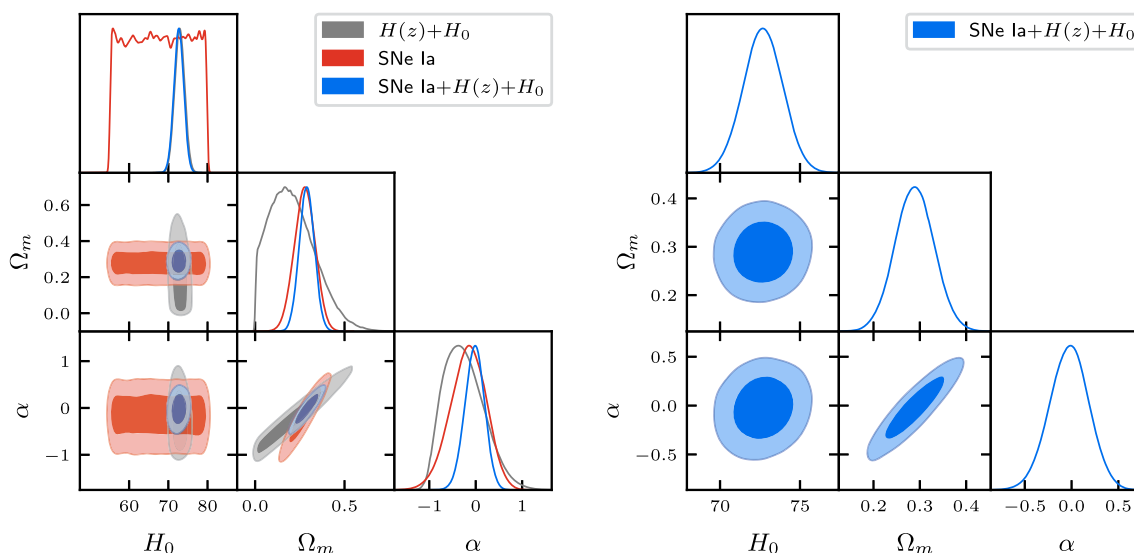
Fig. 6 SNe Ia+$H(z)$+H_0 from SH0ES for $\beta = 0$ (Λ_2 model), at 1 and 2σ c.l., H_0 units are km/s/Mpc. Left: SNe Ia, $H(z)$+SH0ES H_0 and SNe Ia+$H(z)$+SH0ES H_0 constraints. Right: SNe Ia+$H(z)$ joint constraints
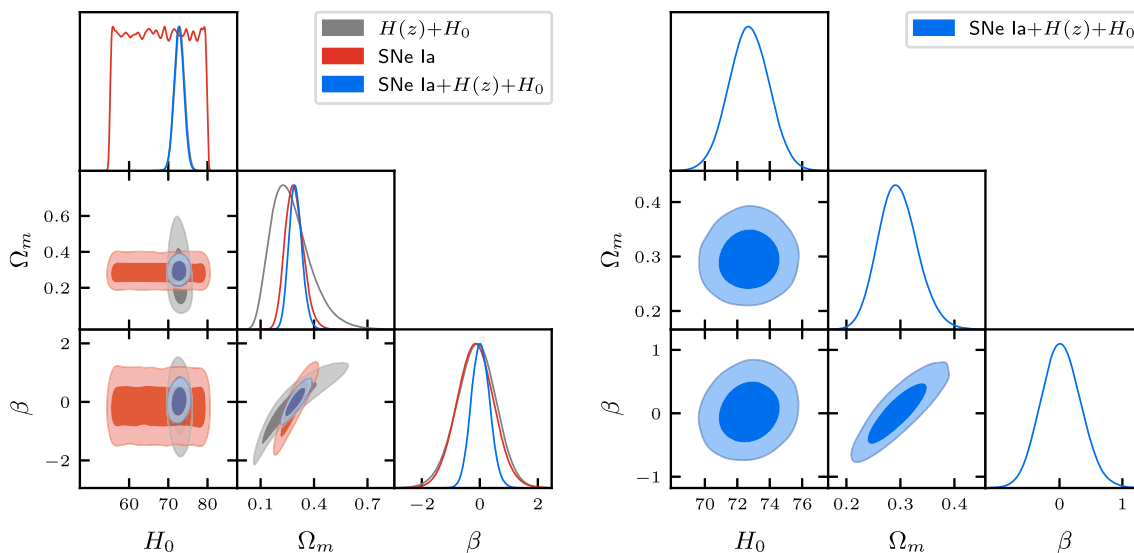
Fig. 7 SNe Ia+$H(z)$+H_0 from SH0ES for $\alpha = 0$ (Λ_3 model), at 1 and 2σ c.l., H_0 units are km/s/Mpc. Left: SNe Ia, $H(z)$+SH0ES H_0 and SNe Ia+$H(z)$+SH0ES H_0 constraints. Right: SNe Ia+$H(z)$ joint constraints

Table 7 SNe Ia+$H(z)$+SH0ES H_0 constraints for $\alpha = 0$ (Λ_3 model)

Parameter	95% limits
H_0 (km/s/Mpc)	$72.7^{+2.5}_{-2.5}$
Ω_m	$0.296^{+0.078}_{-0.069}$
β	$0.03^{+0.65}_{-0.61}$

As one may see from Fig. 8, the interaction term has quite similar behavior to Fig. 4. That is, $\mathcal{Q}(z)$ changes sign for the model Λ_1 and it is negative for models Λ_2 and Λ_3, increasing its absolute value with redshift. However, the best-fit parameters from the analysis with the SH0ES H_0 prior indicate less interaction in the past than in the case with the Planck H_0 prior.

We can see from the figures above, that the most stringent constraints from the data are in the context of the model Λ_3, followed by the constraints over the model Λ_2. While the worst constraints over the parameters are in the case of the model Λ_1. One reason for that is that, as one may see, the contours from SNe Ia and $H(z) + H_0$ are misaligned in the cases Λ_3 and Λ_2 while being aligned in the case of Λ_1. Then, we may say that in the context of the models, Λ_3 and Λ_2, the SNe Ia and $H(z) + H_0$ observations nicely complement each other.

Finally, in order to make a more quantitative comparison among the models analyzed here, we use the Bayesian Information Criterion (BIC) to conclude which model better describes the analyzed data. It is important to mention that the BIC takes into account not only the goodness of fit but also penalizes the excess of free parameters, in agreement with the notion of the *Ockham's razor*. Therefore, BIC favors

simpler models. BIC can be written as [40,41]

$$\text{BIC} = -2 \ln \mathcal{L}_{max} + p \ln N, \tag{42}$$

where N is the number of data, $\mathcal{L}_{max}$ is the maximum of likelihood and p is the number of free parameters. In the model comparison, the model with achieves the lowest BIC is favored. The likelihood has some normalization, such that instead of using the absolute BIC value, what really is important to consider is the relative BIC among models, which is given by

$$\Delta\text{BIC} = -(\text{BIC}_i - \text{BIC}_j). \tag{43}$$

The level of support for each model depends on the value of the ΔBIC and is explained at [42]. As BIC is a model comparison, in Table 8 below, we calculated ΔBIC relative to Λ_3, which has the lowest BIC in the case of the Planck H_0 prior and relative to Λ_2, which has the lowest BIC in the case of the SH0ES H_0 prior. The level of support can be seen in the last column of this table.

We may see that the analysis with the Planck prior over H_0 indicates strong evidence against model Λ_1, while the SH0ES prior indicates moderate evidence against model Λ_1. Both priors, however, can not distinguish between models Λ_2 and Λ_3. We can see that the models Λ_2 and Λ_3 have a better fit in the case of the Planck H_0 prior than in the case of the SH0ES H_0 prior. The situation is inverted, however, in the case of model Λ_1 because the analysis with the Planck H_0 prior discards this model, while the SH0ES H_0 prior has only weak evidence against Λ_1.

Finally, we have analyzed the full $\Lambda(t)$CDM model, as described by Eq. (19). In this case, as it has 1 more free parameter than the subclasses, SNe Ia+$H(z)$+H_0 data were
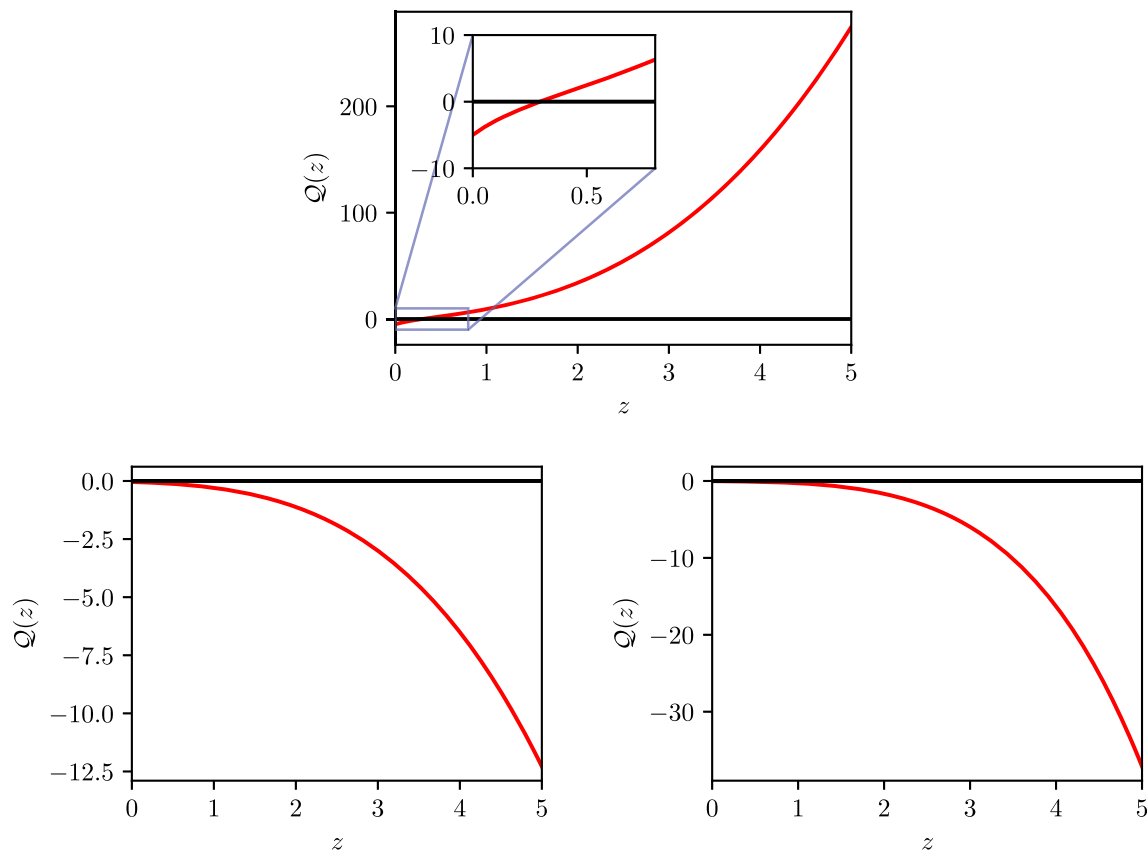
Fig. 8 Interaction term $\mathcal{Q}(z)$ for the best fit parameters from SNe Ia+$H(z)$+SH0ES H_0. Upper panel: $\lambda_* = 0$ (Λ_1 model). Bottom left: $\beta = 0$ (Λ_2 model). Bottom right: $\alpha = 0$ (Λ_3 model)

Table 8 BIC values for the different analysed models, with different H_0 priors. ΔBIC was calculated in comparison with model Λ_3 for each prior, as explained on the text

Model	Data	χ^2_{min}	n_{par}	n_{data}	BIC	ΔBIC	Support
Λ_g	SNe Ia+$H(z)$+Planck H_0	1043.085	4	1080	1071.027	6.984	Decisive
Λ_1 ($\lambda_* = 0$)	SNe Ia+$H(z)$+Planck H_0	1047.614	3	1080	1068.571	4.528	Strong to very strong
Λ_2 ($\beta = 0$)	SNe Ia+$H(z)$+Planck H_0	1043.091	3	1080	1064.048	0.005	Not significant
Λ_3 ($\alpha = 0$)	SNe Ia+$H(z)$+Planck H_0	1043.086	3	1080	1064.043	0.000	Not significant
Λ_g	SNe Ia+$H(z)$+SH0ES H_0	1044.451	4	1080	1072.393	7.333	Decisive
Λ_1 ($\lambda_* = 0$)	SNe Ia+$H(z)$+SH0ES H_0	1046.570	3	1080	1067.527	2.067	Weak
Λ_2 ($\beta = 0$)	SNe Ia+$H(z)$+SH0ES H_0	1044.503	3	1080	1065.460	0.000	Not significant
Λ_3 ($\alpha = 0$)	SNe Ia+$H(z)$+SH0ES H_0	1044.507	3	1080	1065.464	0.004	Not significant

not enough to constrain its free parameters. Then, we choose to work with CMB constraints, in combination with SNe Ia Pantheon and $H(z)$ in order to constrain its free parameters. In order to include the CMB constraints we have used the so called "distance priors" from Planck, as explained in [43]. It includes constraints from Planck over quantities like shift parameter R, acoustic scale l_A and baryon density $\omega_b \equiv \Omega_b h^2$, where $h \equiv \frac{H_0}{100}$. [43] present distance priors in the context of 4 models, namely, ΛCDM, wCDM, ΛCDM+Ω_k and ΛCDM+A_L. As these priors bring strong constraints

from Planck over models which are distinct of $\Lambda(t)$CDM, we choose to work with the prior that yields the weakest constraints, namely, ΛCDM+Ω_k, weakening the prior bias. In order to speed up the convergence of chains, we have chosen to work with baryon density ω_b instead of baryon density parameter Ω_b. The results can be seen on Fig. 9.

As can be seen on Fig. 9, there are strong correlations between the parameters $\alpha - H_0$ and $\alpha - \beta$. One can also see that α and β are strongly constrained by this analysis. More details can be seen on Table 9.
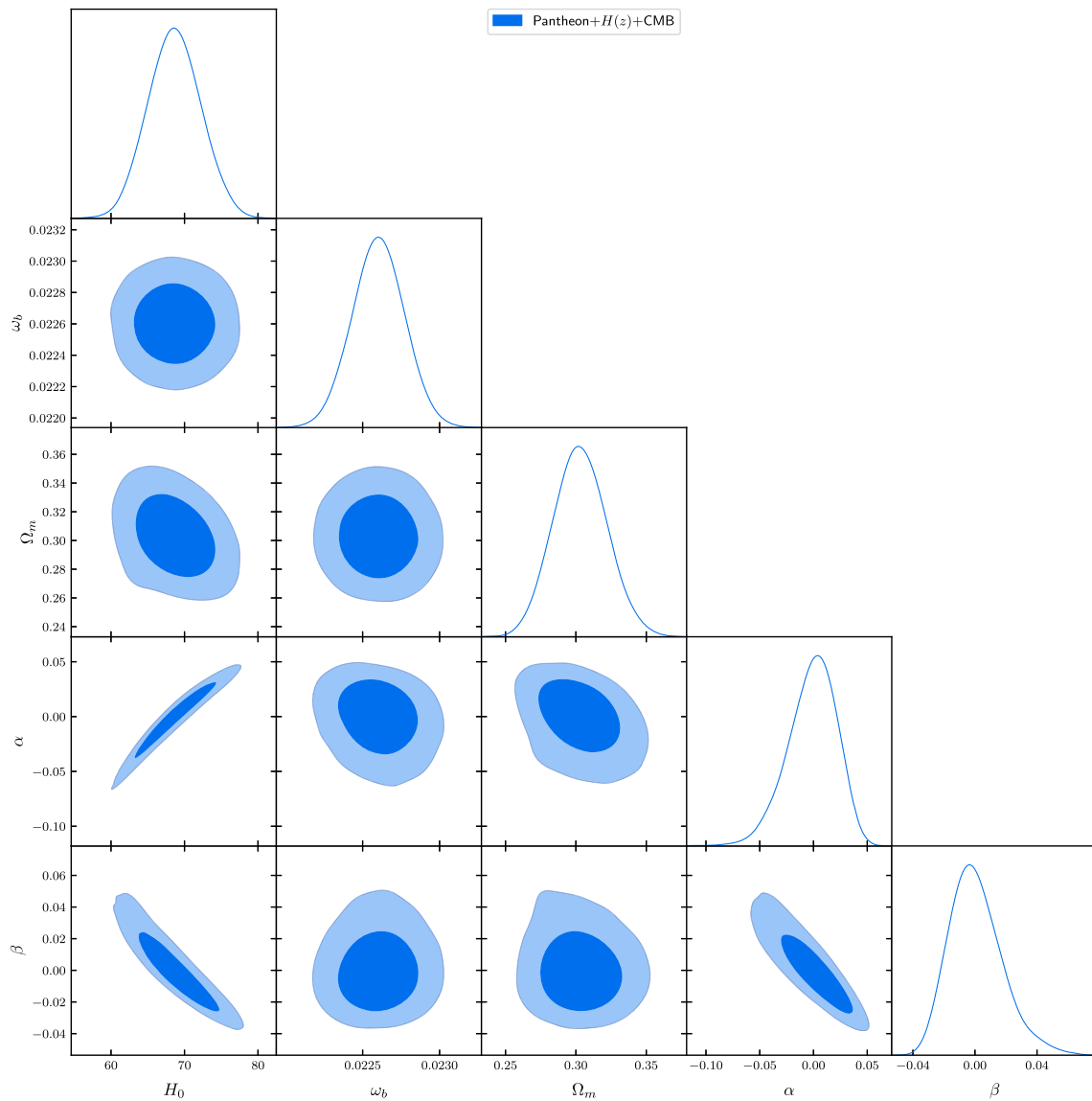
Fig. 9 SNe Ia + $H(z)$ + CMB Planck 2018 distance priors constraints for full Λ_g model, at 1 and 2σ c.l., H_0 units are km/s/Mpc

Table 9 Constraints over Λ_g, Λ_2 and Λ_3 free parameters with 95% limits, from SNe Ia+$H(z)$+CMB

Parameter	Λ_g	Λ_2 $(\beta = 0)$	Λ_3 $(\alpha = 0)$
H_0 (km/s/Mpc)	$68.6^{+7.2}_{-7.0}$	$68.5^{+3.0}_{-2.7}$	$68.6^{+1.7}_{-1.5}$
ω_b	0.02260 ± 0.00034	0.02260 ± 0.00034	$0.02261^{+0.00033}_{-0.00034}$
Ω_m	$0.303^{+0.039}_{-0.037}$	$0.303^{+0.040}_{-0.038}$	$0.303^{+0.036}_{-0.035}$
α	$-0.001^{+0.043}_{-0.047}$	$-0.001^{+0.021}_{-0.022}$	0
β	$0.001^{+0.036}_{-0.033}$	0	$0.000^{+0.017}_{-0.016}$

As can be seen on Table 9, the parameters α and β, which dictate the Λ time dependence, are strongly constrained by CMB, leaving only small windows for Λ variation. In fact, we may see that $-0.048 < \alpha < 0.042$ and $-0.032 < \beta < 0.037$ at 95% c.l. This result has to be read with care, as

we did not make a full CMB power spectrum analysis in the context of $\Lambda(t)$CDM. We have used, instead, distance priors which depend on models where the DM and DE are separately conserved. With that said, the results for the other parameters are similar to the ones obtained from Planck [38]

in the context of ΛCDM, where it was found that $H_0 = 67.4 \pm 0.5$ km/s/Mpc, $\omega_b = 0.0024 \pm 0.0001$ and $\Omega_m = 0.315 \pm 0.007$. This is expected, as the values obtained for α and β are compatible with the ΛCDM model.

In Table 9 we show, for completeness, the results for the subclasses of models which include a bare cosmological constant λ_* term, Λ_2 and Λ_3. As it can be seen, the parameters are in general more constrained in the subclasses than in the general model, which is expected, as they have less free parameters. Again, these results shall be taken with care, as we have used an approximated treatment of the CMB results, but we may conclude that the interaction terms are quite constrained in the context of this analysis.

5 Conclusion

We have analyzed 3 classes of $\Lambda(t)$CDM models against observations of SNe Ia, cosmic chronometers, and priors over the Hubble constant from Planck and SH0ES. We may conclude that 1 class of models, namely, Λ_1, may be discarded by this analysis, mainly in the case of the Planck H_0 prior. In the case of the SH0ES H_0 prior, there is weak evidence against this. Models Λ_2 and Λ_3 can not be distinguished by this analysis.

At this point, it is important to mention that Λ_1 is the only considered model that does not have the standard ΛCDM model as a particular case, once that $\lambda_* = 0$. It seems that the data disfavor $\Lambda(t)$CDM models with this feature, at least for the classes of models analyzed here.

However, as one may see in Tables 2, 3, 5, 4, 6, 7 and Figs. 4 and 8, the current analysis does not discard the possibility of an interaction between pressureless matter and vacuum. We also have seen in the current analysis, that the decaying of pressureless matter into a vacuum is in general favoured against vacuum decay, at least for the recent evolution of the Universe. The Λ_1 model is the only one where this situation changes in the past, allowing for a decay of the vacuum into pressureless matter.

This would indicate an obstacle for the classes of $\Lambda(t)$CDM models analysed here in order to alleviate the cosmological constant problem. On the other hand, a decaying of matter into vacuum may explain why only recently the vacuum density has become non-negligible.

As a final analysis, in the case of the more general model, Λ_g, it was necessary to combine SNe Ia+$H(z)$ with CMB in order to constrain its free parameters. In this case, the Λ time-dependence was quite constrained, but, as we have used an approximate method, a full analysis with the CMB power spectrum is needed in order to give the final verdict about this model.

We emphasize that in the present article, we have assumed the EoS of vacuum to be exactly $w_{vac} = -1$. However, a recent result for the RVM is that the EoS of vacuum evolves with the cosmic history [19]. This would change our results and may be considered in future works.

Further analysis, considering other observational data, such as BAO, growth factor and full CMB power spectrum, in the lines of [23], for instance, in order to better constrain these models should be done in a forthcoming issue.

Data Availability Statement This manuscript has no associated data or the data will not be deposited. [Authors' comment: All the data that has been used in the present work is already available in the quoted literature.]

References

1. L. Perivolaropoulos, F. Skara, New Astron. Rev. **95**, 101659 (2022). arXiv:2105.05208 [astro-ph.CO]
2. A.M. Öztaş, Mon. Not. Roy. Astron. Soc. **481**(2), 2228–2234 (2018)
3. R.G. Vishwakarma, Class. Quantum Gravity **18**, 1159–1172 (2001). arXiv:astro-ph/0012492
4. J.M. Overduin, F.I. Cooperstock, Phys. Rev. D **58**, 043506 (1998). arXiv:astro-ph/9805260
5. H. Azri, A. Bounames, Int. J. Mod. Phys. D **26**(7), 1750060 (2017). arXiv:1412.7567 [gr-qc]
6. H. Azri, A. Bounames, Gen. Relat. Gravit. **44**, 2547–2561 (2012). arXiv:1007.1948 [gr-qc]
7. M. Szydłowski, Phys. Rev. D **91**(12), 123538 (2015). arXiv:1502.04737 [astro-ph.CO]
8. M. Bruni, R. Maier, D. Wands, Phys. Rev. D **105**(6), 063532 (2022). arXiv:2111.01765 [gr-qc]
9. G. Papagiannopoulos, P. Tsiapi, S. Basilakos, A. Paliathanasis, Eur. Phys. J. C **80**(1), 55 (2020). arXiv:1911.12431 [gr-qc]
10. M. Benetti, W. Miranda, H.A. Borges, C. Pigozzo, S. Carneiro, J.S. Alcaniz, JCAP **12**, 023 (2019). arXiv:1908.07213 [astro-ph.CO]
11. M. Benetti, H. Borges, C. Pigozzo, S. Carneiro, J. Alcaniz, JCAP **08**, 014 (2021). arXiv:2102.10123 [astro-ph.CO]
12. I.L. Shapiro, J. Solà, Phys. Lett. B **475**, 236–246 (2000). arXiv:hep-ph/9910462
13. I.L. Shapiro, J. Solà, JHEP **02**, 006 (2002). arXiv:hep-th/0012227

14. I.L. Shapiro, J. Solà, C. Espana-Bonet, P. Ruiz-Lapuente, Phys. Lett. B **574**, 149–155 (2003). arXiv:astro-ph/0303306
15. A. Babic, B. Guberina, R. Horvat, H. Stefancic, Phys. Rev. D **65**, 085002 (2002). arXiv:hep-ph/0111207
16. J. Solà, J. Phys. Conf. Ser. **453**, 012015 (2013). arXiv:1306.1527 [gr-qc]
17. C. Moreno-Pulido, J. Solà, Eur. Phys. J. C **80**(8), 692 (2020). arXiv:2005.03164 [gr-qc]
18. C. Moreno-Pulido, J. Solà Peracaula, Eur. Phys. J. C **82**(6), 551 (2022). arXiv:2201.05827 [gr-qc]
19. C. Moreno-Pulido, J. Solà Peracaula, Eur. Phys. J. C **82**(12), 1137 (2022). arXiv:2207.07111 [gr-qc]
20. C. Moreno-Pulido, J. Solà Peracaula, S. Cheraghchi, Eur. Phys. J. C **83**(7), 637 (2023). arXiv:2301.05205 [gr-qc]
21. J. Solà Peracaula, Phil. Trans. Roy. Soc. Lond. A **380**, 20210182 (2022). arXiv:2203.13757 [gr-qc]
22. J. Solà Peracaula, J. de Cruz Pérez, A. Gomez-Valent, Mon. Not. Roy. Astron. Soc. **478**(4), 4357–4373 (2018). arXiv:1703.08218 [astro-ph.CO]
23. J. Solà Peracaula, A. Gomez-Valent, J. de Cruz Perez, C. Moreno-Pulido, Universe **9**(6), 262 (2023). arXiv:2304.11157 [astro-ph.CO]
24. J. Solà Peracaula, A. Gómez-Valent, J. de Cruz Perez, C. Moreno-Pulido, EPL **134**(1), 19001 (2021). arXiv:2102.12758 [astro-ph.CO]
25. J. Solà Peracaula, J. de Cruz Pérez, A. Gómez-Valent, EPL **121**(3), 39001 (2018). arXiv:1606.00450 [gr-qc]
26. P. Tsiapi, S. Basilakos, Mon. Not. Roy. Astron. Soc. **485**(2), 2505–2510 (2019). arXiv:1810.12902 [astro-ph.CO]
27. N.E. Mavromatos, J. Solà Peracaula, Eur. Phys. J. ST **230**(9), 2077–2110 (2021). arXiv:2012.07971 [hep-ph]
28. J. Solà, A. Gómez-Valent, J. de Cruz Pérez, Astrophys. J. **836**(1), 43 (2017). arXiv:1602.02103 [astro-ph.CO]
29. J.L. Lopez, D.V. Nanopoulos, Mod. Phys. Lett. A **11**, 1–7 (1996). arXiv:hep-ph/9501293
30. W. Chen, Y.S. Wu, Phys. Rev. D **41**, 695–698 (1990). (**erratum: Phys. Rev. D 45, 4728 (1992)**))
31. M. Ozer, M.O. Taha, Phys. Lett. B **171**, 363–365 (1986)
32. M. Ozer, M.O. Taha, Nucl. Phys. B **287**, 776–796 (1987)
33. J.C. Carvalho, J.A.S. Lima, I. Waga, Phys. Rev. D **46**, 2404–2407 (1992)
34. J.A.S. Lima, E.L.D. Perico, G.J.M. Zilioti, Int. J. Mod. Phys. D **24**(04), 1541006 (2015). arXiv:1502.01913 [gr-qc]
35. D.M. Scolnic et al. [Pan-STARRS1], Astrophys. J. **859**(2), 101 (2018). arXiv:1710.00845 [astro-ph.CO]
36. M. Moresco, L. Amati, L. Amendola, S. Birrer, J.P. Blakeslee, M. Cantiello, A. Cimatti, J. Darling, M. Della Valle, M. Fishbach et al., Living Rev. Relat. **25**(1), 6 (2022). arXiv:2201.07241 [astro-ph.CO]
37. R. Sawada, Y. Suwa, Astrophys. J. **908**(1), 6 (2021). arXiv:2010.05615 [astro-ph.HE]
38. N. Aghanim et al. [Planck], Astron. Astrophys. **641**, A8 (2020). arXiv:1807.06210 [astro-ph.CO]
39. E. Di Valentino, O. Mena, S. Pan, L. Visinelli, W. Yang, A. Melchiorri, D.F. Mota, A.G. Riess, J. Silk, Class. Quantum Gravity **38**(15), 153001 (2021). arXiv:2103.01183 [astro-ph.CO]
40. G. Schwarz, Ann. Stat. **6**, 461–464 (1978)
41. A.R. Liddle, Mon. Not. Roy. Astron. Soc. **351**, L49–L53 (2004). arXiv:astro-ph/0401198
42. J.F. Jesus, R. Valentim, F. Andrade-Oliveira, JCAP **09**, 030 (2017). arXiv:1612.04077 [astro-ph.CO]
43. L. Chen, Q.G. Huang, K. Wang, JCAP **02**, 028 (2019). arXiv:1808.05724 [astro-ph.CO]